Ultra-Wideband Transceiver MMIC Tuneable From 74.1 GHz to 147.8 GHz in SiGe Technology

FLORIAN VOGELSANG [1] (Graduate Student Member, IEEE),
JONATHAN BOTT [1] (Graduate Student Member, IEEE), **DAVID STARKE** [1] (Graduate Student Member, IEEE),
CHRISTIAN BREDENDIEK [2] (Member, IEEE), **KLAUS AUFINGER** [3] (Member, IEEE),
AND NILS POHL [1,2] (Senior Member, IEEE)

(Regular Paper)

[1] Institute of Integrated Systems, Ruhr University Bochum, 44801 Bochum, Germany
[2] Fraunhofer Institute for High Frequency Physics and Radar Techniques FHR, 53343 Wachtberg, Germany
[3] Infineon Technologies AG, 85579 Neubiberg, Germany

CORRESPONDING AUTHOR: Florian Vogelsang (e-mail: florian.vogelsang@rub.de).

ABSTRACT   As the use of integrated radar sensors is becoming more common not only in traditional military and automotive but also in medical and industrial applications, the requirements for a radar sensor diversify. For some applications, bandwidth is critical, primarily defining the capability to distinguish targets. Mostly, varying the frequency of an oscillator in the mmWave and THz range is realized by tuning a dc voltage to a variable capacitance. While this is typical for integrated transceivers in silicon-germanium (SiGe) technology, the tunability of a single voltage-controlled oscillator (VCO) limits the bandwidth. This work presents an approach to overcome this limitation by using two simultaneously tuned VCOs combined with a mixer. The oscillators are tuned simultaneously in opposing directions, resulting in an ultra-wideband signal at the mixer's output. The resulting tuning range is the addition of both of the VCOs' respective tuning ranges. The transceiver is realized using the B11HFC SiGe technology, featuring VCOs at center frequencies of 52 GHz and 108 GHz, respectively. The transceivers' output with a center frequency of 111 GHz is continuously tunable over a range of 73.6 GHz (66%). Furthermore, the phase noise contributions from both VCOs along a receiver test are presented.

INDEX TERMS   BiCMOS, differential, FMCW, frequency divider, frequency doubler, frequency-modulated continuous wave, frequency synthesis, high spatial resolution, MMIC, mixer, phase noise, radar, receiver, SiGe, ultra-wideband, voltage-controlled oscillator, VCO.

I. INTRODUCTION

One of the most critical parameters in frequency-modulated continuous wave (FMCW) radar systems is the bandwidth B, which determines the range resolution $\Delta r = c_0/(2 \cdot B)$, where c_0 is the speed of light. Insufficient bandwidth could result in multiple closely positioned targets being detected as a single spatially extended target. However, with increased bandwidth, a precise distinction among all targets becomes achievable without error [1], [2]. This is particularly important for applications like thin sheet measurements [3]. In current research, there are multiple examples of wideband signal generation in SiGe [4], [5], [6], [7], [8], [9], as well as first CMOS systems [10].

In SiGe, the most common wideband signal generation utilizes a single voltage-controlled oscillator (VCO) with a varactor, reaching relative tuning ranges of up to 38.2% and

35.4 GHz in W-band [4]. However, an even larger absolute bandwidth can be achieved at a higher center frequency [9], [11]. While through advancements in SiGe-technologies [12], frequencies up into the THz range become interesting for SiGe circuits, there are some things to consider. According to the free-space path losses,

$$F = \left(\frac{4 \cdot \pi \cdot r \cdot f}{c} \right)^2 \qquad (1)$$

with increasing frequency, the signal attenuation increases. This means the range of the radar is reduced due to the losses as well as the smaller gain of the transistors themselves. Possible ways to achieve higher tuning ranges in lower frequency bands, which are currently in focus for new automotive and 6 G research, are to use direct-digital synthesis (DDS) [5] or to combine multiple [13] or just two VCOs using a mixer [14] [15] while remaining at a lower center frequency despite the high bandwidth.

In this article, the method of mixing two VCOs, in which both VCOs are simultaniously active but detuned differently so that the tuning ranges can be combined, is adapted, resulting in an absolute tuning range of more than 70 GHz at a center frequency just above 100 GHz. At the same time, with frequencies in W- and D-band, flexibility is maintained concerning a system implementation, as for frequencies up to the D-band, bond wires have manageable losses. This creates the possibility of using off-chip antennas on a cheap printed circuit board (PCB).

This work builds upon [16], introducing a more advanced MMIC compared to the previous version. The enhancements include a higher center frequency, a lower phase noise achieved through the revision of one VCO, and a more efficient, compact power amplifier design. Moreover, an additional divider path for advanced circuit stabilization like in [14] is added, as well as a whole receiver path for FMCW radar operation. Concerning measurement results, a particular focus is set on the phase noise of the MMIC. Finally, a verification of the receiver is featured.

The paper is organized as follows: Section II explains the system concept, Section III details the SiGe circuits, which were fabricated using Infineon's B11HFC technology. In Section IV, experimental results of the achieved frequency ranges, output power, and phase noise measurements are presented. In Section V, considerations in context with a full system implementation are discussed. In Section VI, a comparison to previous work is given. A summary of the paper can be found in Section VII.

II. SYSTEM CONCEPT

The main objective of this work is to achieve the highest possible continuous tuning range while using mmWave circuits. When using a traditional approach with a single VCO and subsequent frequency doublers and amplifiers, the maximum achievable tuning range is only related to the VCO's tuning range, thus a varactor in most cases. A possible solution to
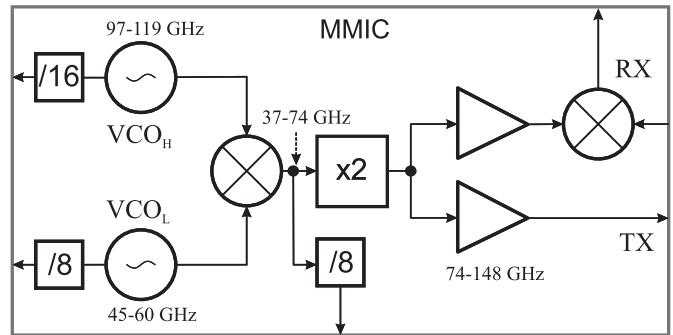
FIGURE 1. Block diagram of the proposed MMIC with two oscillators and full TX/RX paths. Three divider outputs for oscillator stabilization are available.

this is utilizing two VCOs at once. In this case, two oscillators are used and tuned simultaneously, one operating at a higher frequency while the other one is operating at a lower frequency. Both of the outputs are then mixed using a mixer, resulting in the sum and difference frequency being present. From a theoretical perspective, the tuning ranges of two VCOs can be added when mixing both of the VCOs' outputs and using the subtracted or added output [14]. In addition to wideband signal generation, transceiver capabilities are introduced with a receive path and mixer, as well as frequency dividers for advanced frequency synthesis. The block diagram of the system is provided in Fig. 1. In this work, VCO_H has a center frequency of around 108 GHz, while VCO_L is around 52 GHz resulting in a difference frequency of around 56 GHz behind the mixer. To increase the tuning range even further, the mixer is followed by a frequency doubler. To compensate for the losses of the doubler and to guarantee sufficient output power for FMCW measurements as well as the receive mixer, two power amplifier (PA) paths are used, one in the receive path and one in the transmit path.

III. CIRCUIT DESIGN

This section gives a more detailed insight into the circuit design while focusing on the challenges arising from the high tuning range and the mixing concept. The technology used is Infineon's automotive-qualified B11HFC 130 nm SiGe-BiCMOS process [17] with an f_T of 250 GHz and f_{max} of 370 GHz. It features six copper metal layers with MIM-capacitors and an aluminum pad layer. The overall supply voltage of the MMIC is 3.3 V. Only a single divider stage operates at a 5 V supply voltage for performance reasons. All presented circuits operate fully differential. All of the circuit design was carried out using both the Spice-Gummel-Poon and the HICUM-HBT model, together with parasitic extraction, for the most realistic results.

A. VCOS

For the last few years, bipolar LC-based VCOs have proven to be well-suited for wideband signal generation [8], [9]. In

this paper, we use a system design with two different VCO topologies, utilizing the advantages of each of the topologies. The 108 GHz oscillator (VCO$_H$) is realized in a fully differential Colpitts topology. The resonator is based on a pn-varactor Diode C_{var} and a microstrip transmission line L_B, which is used as an inductor. To decouple the oscillators from influences of the load and following circuits, a common base amplifier is used to amplify the generated signal. To achieve even broader tuning ranges, the conventional Colpitts topology can be further enhanced by incorporating an additional varactor, denoted as C_{var}^*, connected to the bases of the core transistors T$_2$. This modified configuration, commonly referred to as the Colpitts-Clapp topology, has demonstrated the capability to attain relative tuning ranges of up to 40% in the E- and W-bands [4], [18].

In addition to the second varactor pair, we have incorporated diode D$_1$ into the tuning voltage input to offset the dc voltage drop across transistor T$_2$. This approach allows for the simultaneous tuning of both varactor pairs within the Colpitts-Clapp topology using a single tuning voltage, denoted as V_{tune}. Furthermore, we have implemented laser fuses at the resonator lines of both voltage-controlled oscillators to mitigate the effects of technology variances and parasitic elements. These laser fuses can be precisely cut using a laser, thereby extending the effective length of the resonator microstrip line and consequently reducing the center frequency of the oscillators.

To enable measurements, such as tuning curves and phase noise measurements, for each VCO individually, frequency dividers (cf. [4]) are connected to both oscillators, which convert the high frequency of the oscillators to a much lower regime, where PCBs and commercial phased-locked-loop (PLL) components are suitable. For the VCO$_L$, a static divide-by-8 is used in emitter-coupled logic (ECL) topology. On the other hand, a static divider in the B11HFC technology is not suitable for VCO$_H$, as the frequency is above 100 GHz [19]. Therefore, an additional first-stage dynamic frequency divider in regenerative topology is utilized, resulting in a divide-by-16 prescaler for VCO$_H$. A schematic of both oscillators is given in Fig. 2. The schematic of the 108 GHz Colpitts VCO$_H$ is visualized in black, while the additions of the 52 GHz Colpitts-Clapp VCO$_L$ are shown in red. Values of the most relevant components for both VCOs are given in Table 1.

B. LO-MIXER AND FREQUENCY DIVIDER

The performance of the entire system concept heavily relies on the LO-mixer, which is responsible for converting the outputs of both VCOs. Therefore, it holds a pivotal role within this MMIC. The requirements regarding compression and linearity are demanding, as two oscillators that are generating high-power signals drive the mixer. Typically, the LO signal has a much higher power than the RF signal. Here, both signals have a level of around 6 dBm, which makes maintaining linear operation of the mixer a big challenge. Therefore, it is prone to generating unwanted harmonics at its output port. The linearity of the mixer was further improved in this work,
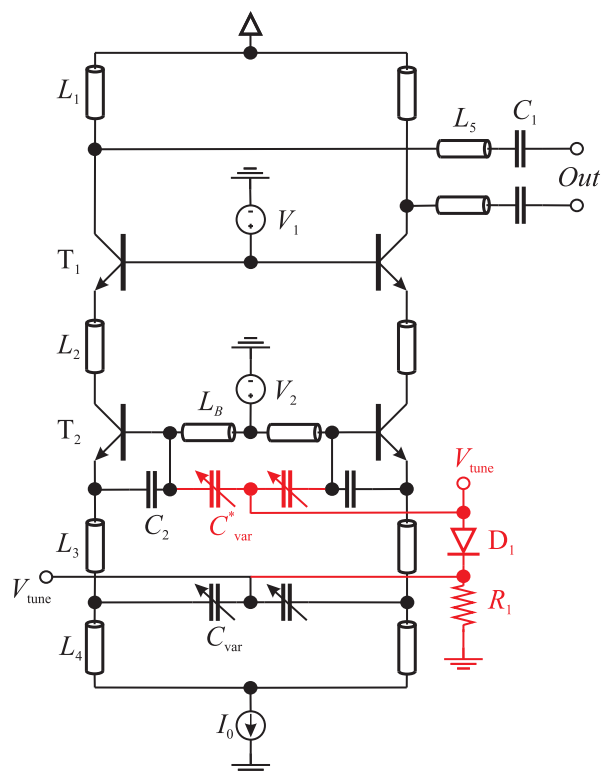

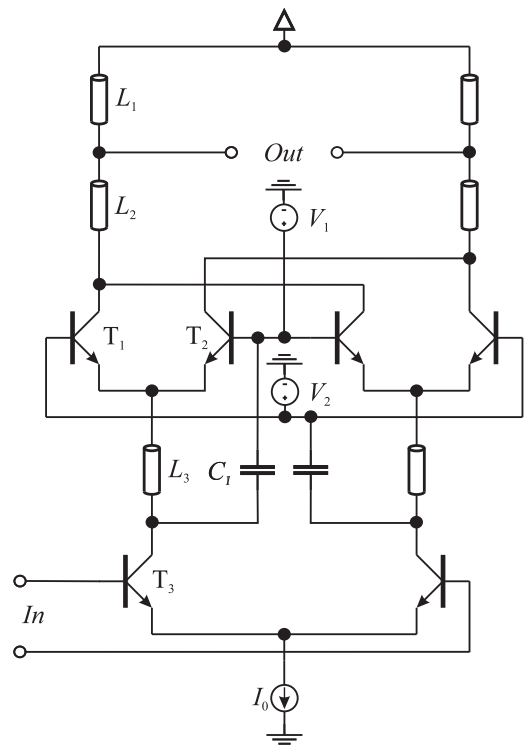**FIGURE 2.** Schematic of VCOs with transmission lines as inductors. (Black: VCO$_H$; Black+Red VCO$_L$). From [16].

TABLE 1. Most Important Component Values for the VCOs. The Transistor Dimension Is the Emitter Length

Component	Value VCO$_H$	Value VCO$_L$
L_1	60 μm	100 μm
L_2	50 μm	45 μm
L_3	30 μm	25 μm
L_4	310 μm	330 μm
L_5	140 μm	180 μm
L_B	78 μm	140 μm
C_1	100 fF	90 fF
C_2	40 fF	40 fF
T$_1$	20 μm	20 μm
T$_2$	20 μm	20 μm

compared to the previous version [16] by redesigning the circuit. While the architecture of the mixer is a traditional Gilbert cell, the difference to typical down-conversion mixers [20] is the load. Usually, a resistive and capacitive load is favored because of its lowpass behavior, which is needed for baseband signals. Since the output frequency range of this mixer reaches up to 74 GHz, a different approach with an inductive load is chosen. The drawback of this is that this favors harmonics close to the targeted output frequency even more. For driving following circuits and loads as well as decoupling the mixer core, there is a subsequent output amplifier within the mixer cell itself. The schematic of the mixer is given in Fig. 3 along with the component values in Table 2.
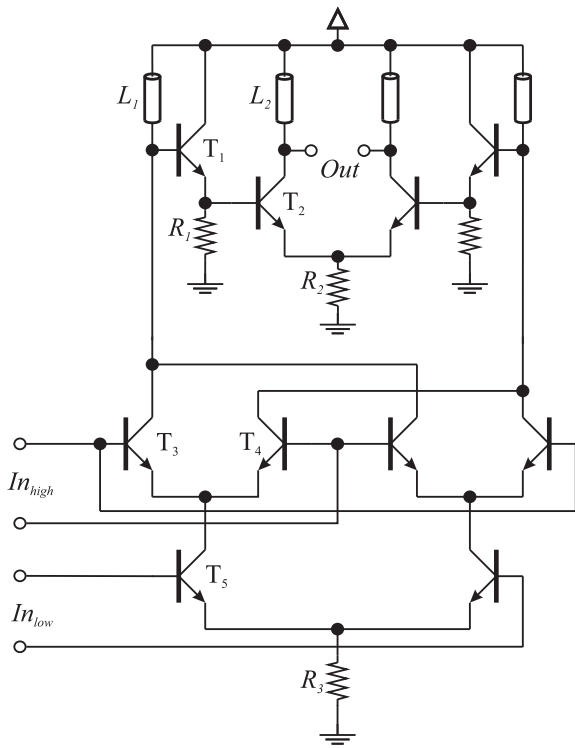
FIGURE 3. Schematic of the mixer with inductive load and integrated buffer. Both of the inputs are connected to a VCO, while the output ranges up to 74 GHz. From [16].

FIGURE 4. Schematic of the bootstrapped gilbert cell doubler. The load is realized with two split up transmission lines, featuring more bandwidth. C_1 is mainly for decoupling the bias from the bases of the upper four transistors.

TABLE 2. Most Important Component Values of the LO Mixer. The Transistor Dimension Is the Emitter Length

Component	Value	Component	Value
L_1	250 μm	T_2	6 μm
L_2	280 μm	$T_3 = T_4$	4.7 μm
T_1	8 μm	T_5	7.5 μm

Subsequent to the mixer, there is a frequency doubler and a frequency divider in parallel. The divider is intended to be used for frequency synthesis within the planned FMCW system. In [14] it is shown that a single output can be sufficient for stabilizing both VCOs simultaneously with the same PLL. Therefore, behind the mixer, a static-divide-by-16 prescaler is used in the same ECL logic as the other dividers but without the need for a dynamic first divider stage. In a later revision of the MMIC, this divider will be the only one persisting to save hardware and, thus, energy.

C. FREQUENCY DOUBLER AND POWER AMPLIFIER

To further enhance the absolute tuning range of the MMIC, the mixer is followed by a frequency doubler, which creates an output signal of up to 148 GHz. The frequency doubler is realized as a Gilbert cell type with bootstrapped modification (similar to [21]) for reduced complexity. One of the drawbacks when using this type of doubler is that the transmission line L_3 (cf. Fig. 4 and Table 3), has a significant influence on the phase difference at the doubler's differential output. This means that

TABLE 3. Most Important Component Values for the Frequency Doubler and the Power Amplifiers. The Transistor Dimension Is the Emitter Length

Doubler			
Component	Value	Component	Value
L_1	80 μm	C_1	150 fF
L_2	45 μm	$T_1 = T_2$	9.4 μm
L_3	190 μm	T_3	11.4 μm
Power amplifier - stage 1			
L_1	80 μm	C_1	400 fF
L_2	60 μm	C_2	230 fF
L_3	80 μm	T_1	14 μm
L_4	100 μm	T_2	11.8 μm
L_5	140 μm		
Power amplifier - stage 2			
L_1	70 μm	C_1	400 fF
L_2	40 μm	C_2	90 fF
L_3	50 μm	T_1	14.8 μm
L_4	20 μm	T_2	14.8 μm
L_5	50 μm		

only for a distinct relative tuning range of around 30–40%, the phase difference will be near 180°. Beyond this relative range, the output power will drop rapidly, limiting the performance of resonant circuits for this special application at the edges of the frequency band. The bootstrapped Gilbert doubler has an inductive load and a core current of about 20 mA. This is quite high for a frequency doubler, but the reason is the following
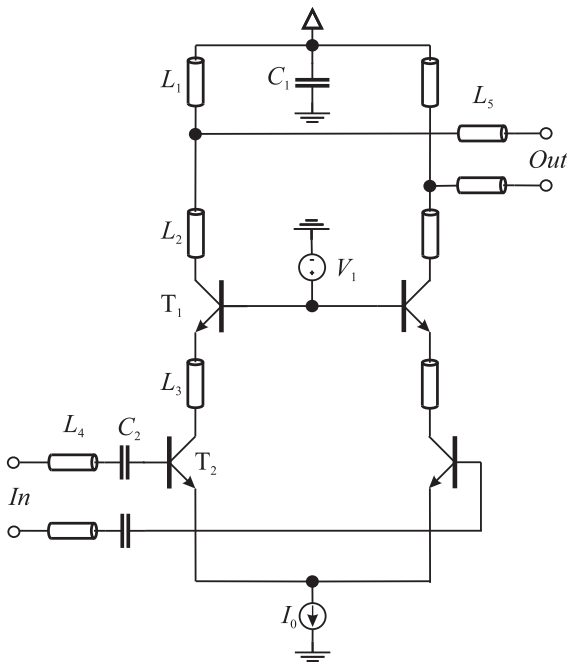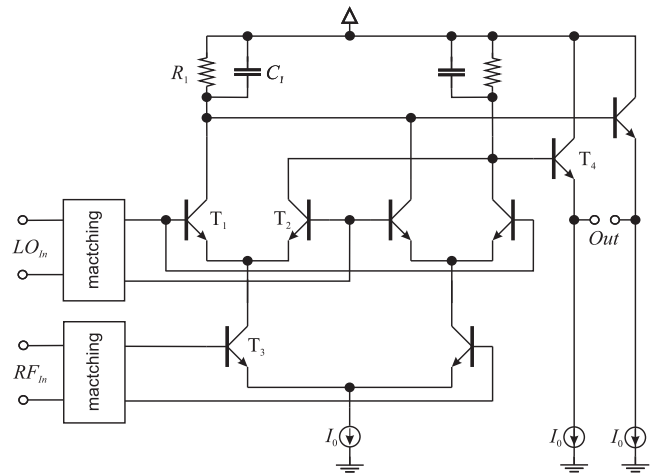
FIGURE 5. Schematic of each of the PA cells. As in the doubler, the load is split up for more bandwidth. C_1 is used to surpress any unwanted signals in virtual ground. In both TX and RX path, two subsequent PAs are used.

FIGURE 6. Schematic of the receive-mixer with emitter follower. The matching networks are optimized for bandwidth, sacrificing some conversion gain.

TABLE 4. Most Important Component Values for the RX Mixer. The Transistor Dimension Is the Emitter Length

Component	Value	Component	Value
R_1	200 Ω	T_3	4 μm
C_1	300 fF	T_4	5 μm
$T_1 = T_2$	3 μm		

load. There are two separate paths subsequent to the doubler, so the conversion gain was designed to be sufficient, peaking at 6 dB, for this load, resulting in the need for more current.

Following the doubler, there are two separate signal paths, each featuring a two-stage power amplifier chain. One path is for transmitting the signal, and the other acts as LO for the receive mixer (cf. Fig. 1). In the previous version [16], a two-path combining approach was used. In this revision of the MMIC, we improved the efficiency of the whole doubler-amplifier chains. While there is still the need for the PAs to work in slightly different frequency ranges due to the limitation of resonant loads, this step is now realized directly within the two subsequent stages rather than in parallel paths. This results in the total number of PA cells being reduced from six to four, but at the cost of some peak output power. Concerning the PA cells themselves, a differential amplifier with a cascode stage is utilized. The schematic is shown in Fig. 5. The transistors operate at the optimal current density for maximum f_T, and the loads' resonance frequency of the subsequent PAs is shifted by around 25% for broadband operation as well as careful interstage matching.

D. RECEIVER
As the MMIC is intended to be used within an FMCW radar system, a receive mixer is needed for coherent measurements. The chosen topology for the mixer is based on a traditional Gilbert cell acting as a fundamental down-conversion mixer with an emitter follower. The main challenge while designing the mixer is keeping the balance between bandwidth, noise,
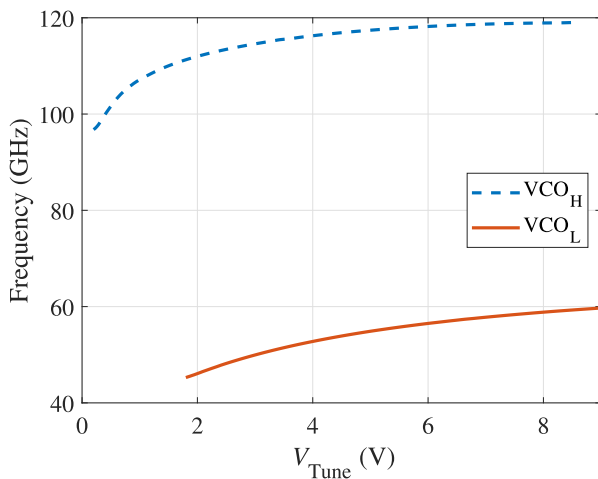
and gain. The schematic of the circuit is presented in Fig. 6, with component values in Table 4. Contrary to the other mixer presented, this receive-mixer uses both a resistive and capacitive load for intermediate signals. The transistors of this mixer are designed to operate a little bit lower than at the optimal current density, as this trades some conversion gain for a lower noise figure. The simulations show a conversion gain of around 4 dB at the center frequency with a noise figure of 14 dB, given a core current of 8.8 mA. Additionally, there are matching networks on both the RF and LO input of the mixer.

IV. MEASUREMENT RESULTS
This section discusses the on-wafer measurements using the SiGe MMIC shown in Fig. 7. As can be seen in the picture, the MMIC offers several off-chip interfaces that are required for measurements and future system integration. On the left side are the dc connections. Positioned on the top and bottom sides are outputs for the three dividers as well as the IF output. The RF interface with transmitter and receiver GSGSG pads are placed on the right, enabling off-chip PCB-based antennas. Since the following measurement results were performed in multiple frequency bands, a short description of each setup will be given within the corresponding paragraph. For all spectral measurements, a Keysight UXA spectrum analyzer was used. For measuring output power, a VDI Erickson PM5B power meter was utilized, while all phase noise results were generated with a Rohde & Schwarz FSWP phase noise analyzer. All measurements are corrected for losses of probes,
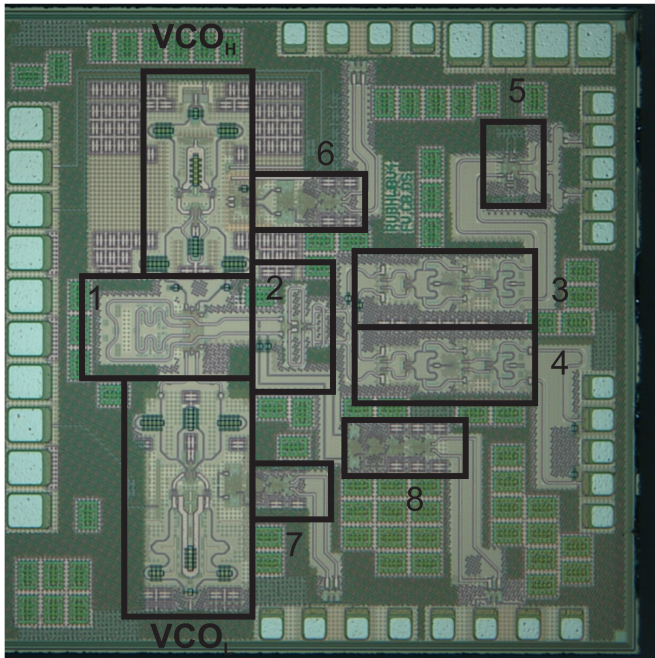
FIGURE 7. Photograph of the MMIC. Size is 1420 x 1448 μm. 1: VCO mixer; 2: Frequency doubler; 3: RX path; 4: TX path; 5: RX mixer; 6: VCO_H divider; 7: VCO_L divider; 8: VCO mixer divider.
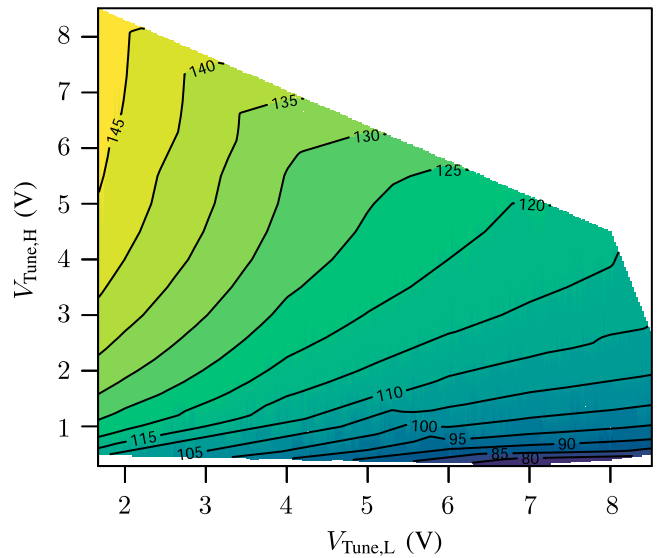

FIGURE 9. Measured, multi-dimensional tuning plot at RF output. $V_{Tune,L}$ is plotted on the x-axis, $V_{Tune,H}$ on the y-axis. Through contour lines and color grading in the plot, the output frequency (in GHz) at the given combination of tuning voltages is displayed.

FIGURE 8. Measured tuning curves of both VCOs. The solid line shows VCO_L, the dashed is VCO_H.

cables, and waveguide tapers. The total dc power consumption of the MMIC is 1354 mW.

A. VCO TUNING CURVES

First of all, the signal generation by the two VCOs is characterized. The tuning curves of both VCOs were measured at the corresponding divider outputs with a direct connection to the spectrum analyzer. The tuning results are shown in Fig. 8. On the bottom, the result for the lower VCO_L is given, showing a tuning range of 14.54 GHz (27.7% rel. tuning range). For VCO_H, a tuning range of 22.27 GHz (20.6%) is reached.

As the results were calculated from the dividers' outputs, no separate VCO output power was obtained, which is also impossible with the current MMIC version, as there are no separate output pads for the VCOs. The frequency dividers themselves are also not available as a breakout, but since the tuning curves and phase noise results for both VCOs are gathered through the dividers, their function is at least proven indirectly.

B. RF OUTPUT

Following the VCO tuning results, the RF output is presented. The spectral results were directly obtained with a spectrum analyzer up until 110 GHz with a corresponding 1 mm coax cable and GSG probe. Results above 110 GHz were captured using an additional VDI spectrum analyzer extender and a corresponding GSG 170 GHz WR 6.5 waveguide probe. For power measurements below 110 GHz, a coax-to-waveguide transition was used in combination with the PM5B. Other than that, the PM5B was directly connected to the WR 6.5 probe with a taper. The first result presented is the output tuning curve. Since this is a multidimensional problem due to the two different tuning voltages, a 3D plot is given in Fig. 9. In the plot, the frequency is visualized through marked contour lines, as well as color grading, where purple is the lowest and yellow the highest frequency. The output signal can be tuned from 74.16 GHz up to 147.8 GHz, resulting in a continuous tuning range of 73.63 GHz (66%). When incorporating the results from the VCOs, a theoretical range of

$$2 \cdot (14.54 + 22.27)\,\text{GHz} = 36.81\,\text{GHz} \cdot 2 = 73.62\,\text{GHz}$$

is possible. This shows that the output frequency range is not limited by the system architecture or individual circuits,
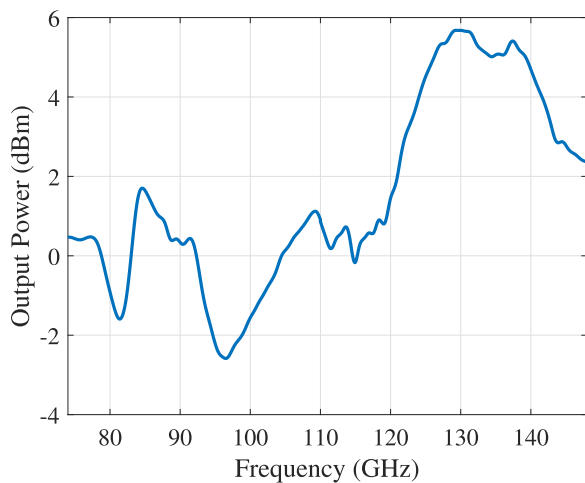
FIGURE 10. Measured differential output power over whole range, combining *W*- and *D*-band results. Overall, a variation of around 8 dB can be observed, while the power peaks at 5.7 dBm.

FIGURE 11. Exemplary measured output spectrum at 105 GHz with *W*-band equipment. The peak is around 105 GHz and is 20 dB stronger than the spurs.


FIGURE 12. Exemplary measured output spectrum at 128 GHz with *D*-band equipment. Spurs are rejected by 21 dB.

but reaches the theoretical limit set by the tuning ranges of the two VCOs. The differential output power is shown in Fig. 10. Note there is a small jump at 110 GHz due to the change in equipment, resulting in a small difference through imperfections in the measurement setup and correction. Furthermore, between 110 and 120 GHz there is a fluctuation in the measured output power. The main reason for this is the fact that this frequency range can be achieved using a huge amount of different VCO-frequency combinations, as it is quite close to the center frequency. On the other hand, since it's on the lower edge of the WR 6.5 equipment, there may be some resonance occurring here, which is not present in the coax-based measurement. Overall, the variation of output power is around 8 dB, which, given the high tuning range, is moderate. The peak power is 5.7 dBm and is comparable to other published work [22], [23] for radar purposes.

Another important result when talking about mixing approaches is the spectral purity of the mixed signal, as it is very prone to have multiple harmonics in it, which could lead to ghost targets in FMCW measurements [24]. Therefore, in Figs. 11 and 12, the output spectra at two exemplary points in the *W*- and *D*-band are given. The source of the spurs is most likely the LO mixer itself. The mixer is fed with two strong (∼6 dBm) signals from the VCOs, which drives the mixer deep in saturation, where nonlinear effects cause harmonic frequencies. The subsequent frequency doubler is also based on a Gilbert cell, in which all of the now-present frequencies are mixed again. Furthermore, in the *D*-band measurement setup, the extender modules' LO frequency, which is around 5 GHz, may be present as a mixing product with the MMIC signal. Compared to [16], the harmonic suppression is slightly improved and is around 20 dB for the *W*-band and 21 dB in the *D*-band, respectively. This value is also dependent on
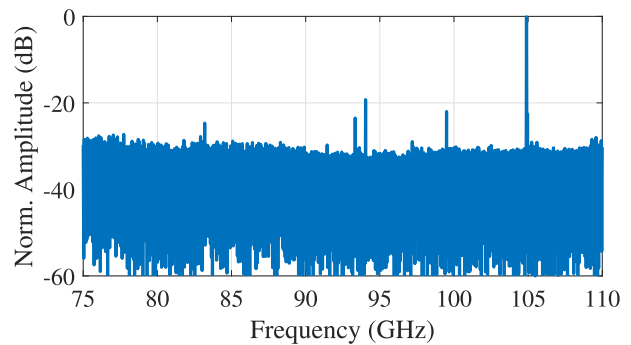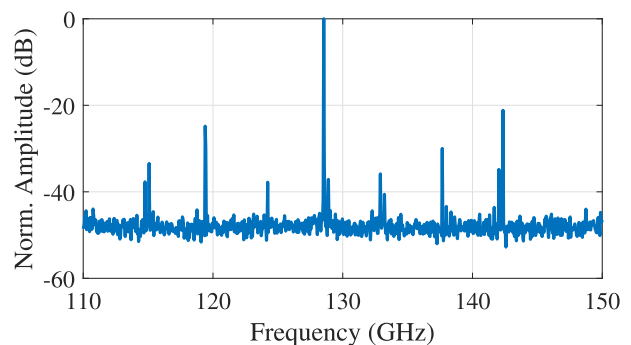
the chosen combination of tuning voltages, which has to be considered during system design to avoid errors in FMCW operation.

C. PHASE NOISE RESULTS

In this part, the phase noise results of the different outputs are discussed. Generally, three measurements were performed at the three corresponding divider outputs. For this, a Rohde & Schwarz FSWP was directly connected to the outputs with a GS probe and cable. In Fig. 13, the results for both oscillators are presented for an offset frequency of 1 MHz. Note that the noise was measured at the divider outputs and corrected for the frequency division to represent the actual noise at the corresponding VCO. As to be expected, the noise of VCO$_H$ is worse due to its higher frequency, while for $V_{tune,H} > 8.3$ V, the noise worsens due to the beginning of a varactor breakthrough. VCO$_H$ reaches values of up to -90 dBc/Hz, VCO$_L$ -97 dBc/Hz, respectively. The frequency-dependent phase noise at the mixer output is given in Fig. 14, reaching -88 dBc/Hz at its best. In the plot, one can see several peaks. The peaks at the edges are caused by the beginning breakthrough of the VCOs' varactors, while the other peaks are most likely just measurement artifacts. A possible explanation is that at these frequencies, the spurs
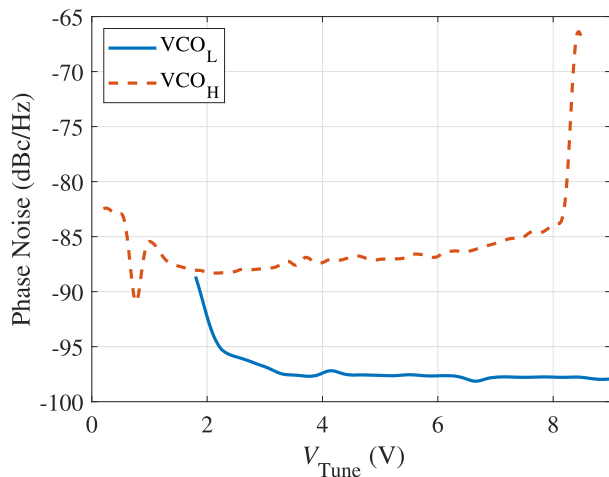
FIGURE 13. Measured phase noise of both VCOs vs. tuning voltage at 1 MHz offset. Note that the frequency of the oscillators differ, hence they have different levels.
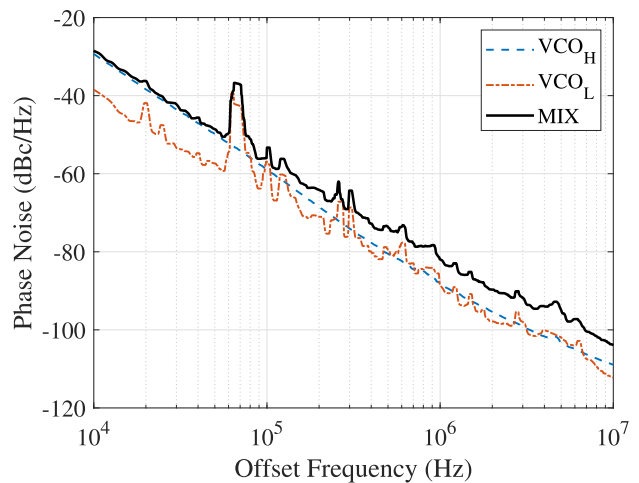

FIGURE 15. Phase noise vs. offset frequency for $V_{Tune,H} = 2$ V, $V_{Tune,L} = 3$ V and mixer output, normalized to 100 GHz. It is worth noting that the resulting noise is roughly the sum of both VCOs' noise, as it follows the shape really closely.

FIGURE 14. Measured phase noise at mixer output vs. frequency. There are several measurement artifacts within the plot, that show unrealistic peaks. Only the peaks at the very edges are correct due to varactor breakthrough.

FIGURE 16. Photograph of the measurement setup for receiver testing. Left: VNA-X with WR 6.5 GSG probe; Bottom: GSSG RX mixer output; Top: VCO mixer divider output; Right: DC supply.

are a bit stronger than elsewhere and close to the carrier, influencing the sensitive phase noise measurement with the phase noise analyzer. Since all three of the presented values are taken at different frequencies for a given measurement point, normalization is performed. In this case the frequencies are $f_{VCO,H} = 111.5$ GHz and $f_{VCO,L} = 50$ GHz, resulting in $f_{MIX} = 61.5$ GHz. The noise at all three outputs, normalized to an output frequency of 100 GHz, is plotted over the offset frequency in Fig. 15. The solid line is the mixer output. Careful investigation of the presented measurements leads to the conclusion that the resulting phase noise after mixing both VCOs roughly follows the sum of the VCOs. Below 5.7 kHz, VCO$_H$ dominates, while beyond this point, VCO$_L$ defines the shape of the output noise. To the author's best knowledge, this is the first time that this was demonstrated for a VCO mixing system concept in detail, as previous work [14] only showed the resulting noise. All in all, this proves that the drawback of the huge tuning range is an increased phase noise, although it is not a showstopper.

D. RECEIVER
As the final measurement, the receiver path of the MMIC is tested. For this, a Keysight PNA-X vector network analyzer, extended to the *D*-band with a VDI VNA extender module, is used to generate an artificial receive signal and feed it into the receive-mixer. This is done single-ended only due to the lack of a balun, while the mixer input is differential in normal operation. Simultaneously, the LO-mixer divider output was checked with a spectrum analyzer to determine the exact LO frequency. A picture of the setup is depicted in Fig. 16. To obtain the baseband IF-signal, a Keysight oscilloscope was used, probing differentially. The receiver tests were conducted at different frequencies, but to save redundancy, the IF-signal, as well as the associated spectrum, is given in Fig. 17 for $f_{RF} = 122$ GHz. The IF signal is around 470 MHz with an amplitude of 200 mV, as the oscillator is tuned to an offset compared to the RF frequency. In this case, the output power of the VNA-X was set to its maximum, resulting in an RF power of 7.5 dBm on the chip. Since no measurement was conducted for the conversion gain due to a lack of de-embedding precision (pads, no RX balun), simulation

(a)

(b)
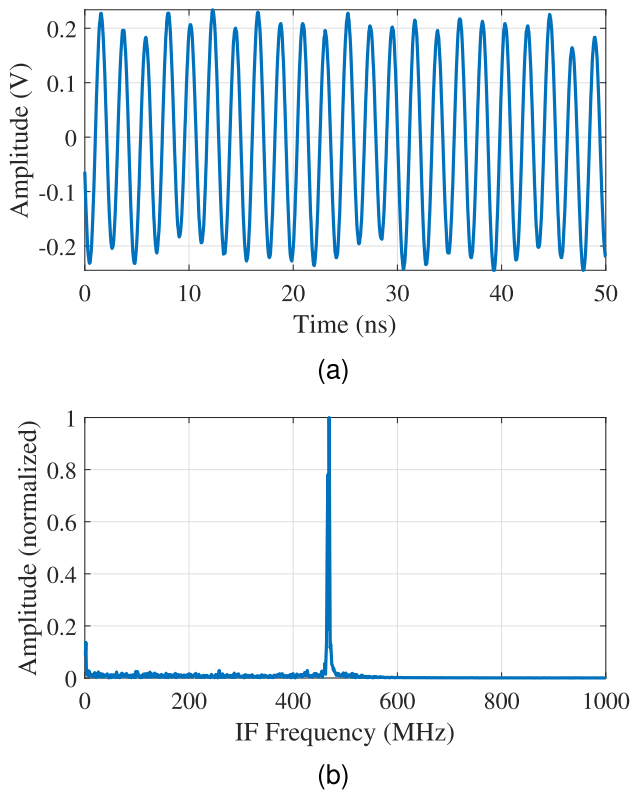
FIGURE 17. Measured time signal at the IF output (a) and corresponding spectrum (b) for $V_{Tune,H}$ = 5 V and $V_{Tune,L}$ = 6 V, resulting in an RF frequency of f_{RF}=122 GHz. The RF input signal into the mixer was chosen to be at an 470 MHz frequency offset.
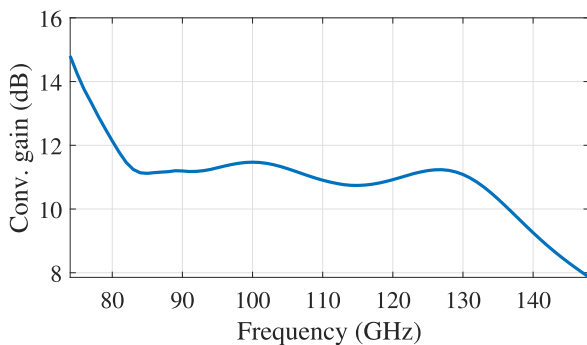
FIGURE 18. Simulated conversion gain of the RX mixer across the combined tuning range of both VCO$_H$ and VCO$_L$.

data is given in Fig. 18. It shows a conversion gain of 11 dB in the center of the tuning range. In summary, the MMIC demonstrated its suitability for the intended wideband FMCW radar measurements.

V. SYSTEM CONSIDERATIONS
In this section, the antenna design, as well as the PLL design for the planned FMCW-radar sensor, are discussed.

When designing a system with this high tuning range, antenna design is one of the main challenges. Since there is no antenna integrated on the MMIC, an off-chip solution is required. Traditional concepts like patch antennas are typically limited in relative bandwidth due to the resonance used. Concepts like Vivaldi antennas can be used to overcome this issue. A lot of published work demonstrates high relative bandwidths up to 186% on different substrates [25], [26], [27]. Therefore, this concept is the most suitable for this system. Moreover, the off-chip transition is a challenging task as well, as it may introduce losses and the need for bond-wire compensation. Yet, there are promising approaches [28], [29]. However, the design of the antenna for this system still has to be performed since this work is focused on the MMIC itself.

For frequency synthesis in the system, the approach presented in [14], [30] is planned to be used. In this concept, both VCOs are stabilized using the mixed output only. This greatly reduces the complexity of the necessary PLL design. An advantage of this concept for two VCOs is that it flattens the tuning steepness (K_{VCO}) across the tuning range compared to a single VCO if one of the tuning voltages is inverted and slightly shifted. This results in the VCO being tuned against each other, forming the flatter KVCO through superpositioning. This makes designing a PLL and frequency control much more convenient.

Concerning phase noise performance, it is clear that this concept's phase noise is always worse than a single VCO due to the system principle. The reason for this is that when mixing both VCOs, the phase noise is added and dominated by the worse one. Since there is a subsequent frequency doubler after the mixer, the noise at the output will worsen by another 6 dB due to the frequency translation of the doubler. While this may be a problem in the system's noise performance in long-range applications, for the target application scenarios, which are limited in range (e.g., a few meters), the noise correlation helps to mitigate the effect of the higher phase noise within short-range [31].

VI. COMPARISON
In this section, the measured results are compared to state-of-the-art transmitters and transceivers. A corresponding table is given in Table 5. In previously published work, mostly a single VCO is used to generate the signal. This results in relative tuning ranges of up to 39% while showing good phase noise results and output power as well. Additionally, there is some work that utilizes two VCOs to profit from the much higher tuning range in the frequency regime below 60 GHz. This proposed work shifts the center frequency above 100 GHz, exhibiting the largest tuning range and, thus, the best target separation capabilities within this frequency range while also featuring a receiver. The drawback of this approach can be seen in the phase noise results, which are slightly worse than single VCO results due to the system concept itself as well as the frequency.

TABLE 5. State-of-the-Art Wideband Transmitters and Transceivers Around 100 GHz

Ref.	Tech.	Type	f_c (GHz)	Tuning Range (GHz)	rTR (%)	P_{dc} (mW)	P_{Out} (dBm)	Phase Noise (dBc/Hz) at 1 MHz offset
[4]	130 nm	Colpitts-Clapp VCO (TX)	91.8	74.0 − 109.5	38.6	215	7	−81...93
[32]	130 nm	VCO with multipliers (TX)	62.2	37.0 − 87.0	81.0	241	3	−70...95
[15]	130 nm	Dual VCO with mixer (TX/RX)	26	6.0 − 46.0	154	−	−	−
[33]	350 nm	Colpitts VCO (TX)	90.5	78.0 − 91.0	11.6	60	4.6	−94...112♣
[34]	130 nm	FMCW transceiver (TX/RX)	148	121.5 − 174.5	35.8	2200	8	−
[9]	90 nm	Colpitts-Clapp VCO (TX)	90	78.7 − 102.8	26.6	95.7	6.4	−67...78
[16]	130 nm	Dual VCO Signal Source (TX)	114	86.0 − 142.0	49	1340	8	−
[18]	350 nm	Colpitts-Clapp VCO (TX)	81	68.8 − 93.3	30	240	12	−91...97
[35]	130 nm	FMCW transceiver (TX/RX)	240	207.0 − 247.0	17	3500	−	−
[36]	16 nm FinFET	Harmonic oscillator (TX)	126	108.7 − 120.6	22.5	40.9	2	−103...111♣
[22]	130 nm	FMCW transceiver (TX/RX)	154	126.0 − 182.0	36.4	1000	−8	−80.0♠
[37]	130 nm	FMCW transceiver (TX/RX)	96	83.0 − 109.0	27	850	19.7	−90...94
This	130 nm	Dual VCO transceiver (TX/RX)	111	74.16 − 144.8	66.0	1354	5.7	−76...82

Note: ♣ : at 10 MHz, ♠ : at 10 kHz, in PLL loop

VII. CONCLUSION

In this work, we presented an ultra-wideband transceiver MMIC in SiGe technology. The concept is based on two VCOs that are mixed and multiplied. The total achievable continuous tuning range is 73.63 GHz at a center frequency of 111 GHz, resulting in 66% relative tuning range. The measured peak output power is 5.7 dBm, which is comparable to other published work for radar purposes, while the high tuning range enables a high-resolution measurement sensor distinguishing distance difference of down to 2 mm. To the authors' best knowledge, this is the highest reported continuous tuning range for this frequency band, covering both WR10 and WR8 waveguide bands, as well as the first time detailed phase noise analysis for VCO mixing concepts is performed. In future work, a sensor can be implemented with this presented MMIC with advanced frequency synthesis capabilities, where only one divider output is used to stabilize both oscillators in a single PLL.

ACKNOWLEDGMENT

REFERENCES

[1] S. Olbrich and C. Waldschmidt, "Optimization of target separation capability for FMCW radar systems," in *Proc. IEEE MTT-S Int. Conf. Microw. Intell. Mobility*, 2018, pp. 1–4.

[2] S. Xu and A. Yarovoy, "Motion-based separation and imaging of closely spaced extended targets," *IEEE Sensors J.*, vol. 20, no. 22, pp. 13542–13551, Nov. 2020.

[3] S. Mann et al., "High-precision interferometric radar for sheet thickness monitoring," *IEEE Trans. Microw. Theory Techn.*, vol. 66, no. 6, pp. 3153–3166, Jun. 2018.

[4] C. Bredendiek, K. Aufinger, and N. Pohl, "Full waveguide E- and W-band fundamental VCOs in SiGe: C technology for next generation FMCW radars sensors," in *Proc. IEEE 14th Eur. Microw. Integr. Circuits Conf.*, 2019, pp. 148–151.

[5] J.-B. Yan et al., "Ultrawideband FMCW radar for airborne measurements of snow over sea ice and land," *IEEE Trans. Geosci. Remote Sens.*, vol. 55, no. 2, pp. 834–843, Feb. 2017.

[6] D. Kissinger, "D-band and terahertz frontends for 6G wireless communications in SiGe BiCMOS technologies," in *Proc. IEEE MTT-S Int. Wireless Symp.*, 2022, pp. 1–3.

[7] N. Sarmah, P. R. Vazquez, J. Grzyb, W. Foerster, B. Heinemann, and U. R. Pfeiffer, "A wideband fully integrated SiGe chipset for high data rate communication at 240 GHz," in *Proc. IEEE 11th Eur. Microw. Integr. Circuits Conf. (EuMIC)*, 2016, pp. 181–184.

[8] Y. Shan, Y. Liang, C. Li, W. Sun, and Z. Fang, "Review of recent progress on solid-state millimeter-wave and terahertz signal sources," *Int. J. Circuit Theory Appl.*, vol. 52, no. 1, pp. 439–472, Jul. 2023.

[9] D. Starke, F. Vogelsang, J. Wittemeier, C. Bredendiek, K. Aufinger, and N. Pohl, "Fully differential 90 GHz and 180 GHz signal sources with tuning ranges of 24.1 GHz and 51.7 GHz in 90 nm SiGe-BiCMOS," in *Proc. IEEE 6th Int. Workshop Mobile THz Syst.*, 2023, pp. 1–5.

[10] P. Zhou, H. Gao, J. Sun, L. Peng, J. Chen, and W. Hong, "A 120 GHz transmitter for high resolution radar application in 40 nm CMOS," in *Proc. IEEE MTT-S Int. Wireless Symp.*, 2022, pp. 1–3.

[11] C. Bredendiek, N. Pohl, T. Jaeschke, K. Aufinger, and A. Bilgic, "A 240 GHz single-chip radar transceiver in a SiGe bipolar technology with on-chip antennas and ultra-wide tuning range," in *Proc. IEEE Radio Freq. Integr. Circuits Symp.*, 2013, pp. 309–312.

[12] P. Chevalier et al., "SiGe BiCMOS current status and future trends in Europe," in *Proc. IEEE BiCMOS Compound Semicond. Integr. Circuits Technol. Symp.*, 2018, pp. 64–71.

[13] T. Drechsel, N. Joram, and F. Ellinger, "An ultra-wideband 3-23 GHz VCO array with high continuous tuning range for FMCW radar application," in *Proc. IEEE 12th German Microw. Conf.*, 2019, pp. 103–106.

[14] T. T. Braun, J. Schöpfel, A. J. M. M., and N. Pohl, "Achieving a relative bandwidth of 176% with a single PLL at up to 12.5 GHz," in *Proc. IEEE 52nd Eur. Microw. Conf.*, 2022, pp. 127–130.

[15] B. Welp, G. Briese, and N. Pohl, "Ultra-wideband FMCW radar with over 40 GHz bandwidth below 60 GHz for high spatial resolution in SiGe BiCMOS," in *Proc. IEEE/MTT-S Int. Microw. Symp.*, 2020, pp. 1255–1258.

[16] F. Vogelsang, D. Starke, J. Wittemeier, C. Bredendiek, K. Aufinger, and N. Pohl, "Ultra-wideband signal source tuneable from 86 GHz to 142 GHz in SiGe technology," in *Proc. IEEE 6th Int. Workshop Mobile Terahertz Syst.*, 2023, pp. 1–5.

[17] J. Böck et al., "SiGe HBT and BiCMOS process integration optimization within the DOTSEVEN project," in *Proc. IEEE Bipolar/BiCMOS Circuits Technol. Meeting*, 2015, pp. 121–124.

[18] N. Pohl, H.-M. Rein, T. Musch, K. Aufinger, and J. Hausner, "SiGe bipolar VCO with ultra-wide tuning range at 80 GHz center frequency," *IEEE J. Solid-State Circuits*, vol. 44, no. 10, pp. 2655–2662, Oct. 2009.

[19] V. Issakov, S. Trotta, and H. Knapp, "Low-voltage flip-flop-based frequency divider up to 92-GHz in 130-nm SiGe BiCMOS technology," in *Proc. IEEE Integr. Nonlinear Microw. Millimetre-Wave Circuits Workshop*, 2017, pp. 1–3.

[20] C.-S. Lin, P.-S. Wu, H.-Y. Chang, and H. Wang, "A 9-50-GHz gilbert-cell down-conversion mixer in 0.13 μm CMOS technology," *IEEE Microw. Wireless Compon. Lett.*, vol. 16, no. 5, pp. 293–295, May 2006.

[21] S. Kueppers, K. Aufinger, and N. Pohl, "A fully differential 100–140 GHz frequency quadrupler in a 130 nm SiGe: C technology for MIMO radar applications using the bootstrapped gilbert-cell doubler topology," in *Proc. IEEE 17th Topical Meeting Silicon Monolithic Integr. Circuits RF Syst.*, 2017, pp. 37–39.

[22] S. Kueppers, T. Jaeschke, N. Pohl, and J. Barowski, "Versatile 126182 GHz UWB D-band FMCW radar for industrial and scientific applications," *IEEE Sens. Lett.*, vol. 6, no. 1, pp. 1–4, Jan. 2022.

[23] N. Pohl, T. Jaeschke, S. Kuppers, C. Bredendiek, and D. Nusler, "A compact ultra-wideband mmWave radar sensor at 80 GHz based on a SiGe transceiver chip (focused session on highly-integrated millimeter-wave radar sensors in SiGe BiCMOS technologies)," in *Proc. IEEE 22nd Int. Microw. Radar Conf.*, 2018, pp. 345–347.

[24] S. Thomas, C. Bredendiek, and N. Pohl, "A SiGe-based 240-GHz FMCW radar system for high-resolution measurements," *IEEE Trans. Microw. Theory Techn.*, vol. 67, no. 11, pp. 4599–4609, Nov. 2019.

[25] J. Yin, J. Li, D. Tan, H. Zhai, and W. Zhong, "An ultra-wideband miniaturized dual-polarized vivaldi antenna," in *Proc. IEEE Int. Appl. Comput. Electromag. Soc. (ACES-China) Symp.*, 2021, pp. 1–2.

[26] H. F. Hammad, "UWB modified elliptical antipodal Vivaldi antenna array fed with four stage wilkinson power divider," in *Proc. IEEE Int. Symp. Antennas Propag. USNC-URSI Radio Sci. Meeting*, 2019, pp. 463–464.

[27] X. Shi, Y. Cao, Y. Hu, X. Luo, H. Yang, and L. H. Ye, "high-gain antipodal Vivaldi antenna with director and metamaterial at 1–28 GHz," *IEEE Antennas Wireless Propag. Lett.*, vol. 20, no. 12, pp. 2432–2436, Dec. 2021.

[28] P. V. Testa, C. Carta, and F. Ellinger, "Novel high-performance bond-wire chip-to-chip interconnections for applications up to 220 GHz," *IEEE Microw. Wireless Compon. Lett.*, vol. 28, no. 2, pp. 102–104, Feb. 2018.

[29] J. Ding, X. Shang, C. Buck, M. Geen, and N. Ridler, "Low-loss 140-175 GHz MMIC-to-waveguide transitions and MMIC-to-MMIC interconnections," in *Proc. IEEE 51st Eur. Microw. Conf.*, 2022, pp. 91–94.

[30] T. T. Braun, J. Schoepfel, A. J., M. M., and N. Pohl, "Overcoming the relative bandwidth limitations of single VCO frequency synthesizers by implementing a novel PLL architecture," *Int. J. Microw. Wireless Technol.*, pp. 1–10, 2024, doi: 10.1017/S1759078723001484.

[31] K. Siddiq, R. J. Watson, S. R. Pennock, P. Avery, R. Poulton, and B. Dakin-Norris, "Phase noise analysis in FMCW radar systems," in *Proc. IEEE Eur. Radar Conf.*, 2015, pp. 501–504.

[32] C. Bredendiek, F. Vogelsang, K. Aufinger, and N. Pohl, "A 37-87 GHz continuously tunable signal source in a 130 nm SiGe: C BiCMOS technology," in *Proc. IEEE 17th Eur. Microw. Integr. Circuits Conf.*, 2022, pp. 276–279.

[33] E. Vardarli, M. Müller, and M. Schröter, "A W-band SiGe-HBT colpitts VCO for millimeter-wave applications with an analog tuning range of 12%," in *Proc. IEEE 22nd Topical Meeting Silicon Monolithic Integr. Circuits RF Syst.*, 2022, pp. 81–84.

[34] S. Hansen, C. Bredendiek, G. Briese, and N. Pohl, "D-band FMCW radar sensor for industrial wideband applications with fully-differential MMIC-to-RWG interface in SIW," in *Proc. IEEE MTT-S Int. Microw. Symp.*, 2021, pp. 815–818.

[35] S. Thomas, C. Bredendiek, T. Jaeschke, F. Vogelsang, and N. Pohl, "A compact, energy-efficient 240 GHz FMCW radar sensor with high modulation bandwidth," in *Proc. IEEE German Microw. Conf.*, 2016, pp. 397–400.

[36] B. Philippe and P. Reynaert, "A 126 GHz, 22.5% tuning, 191 dBc/Hz FOMt 3rd harmonic extracted class-F oscillator for D-band applications in 16 nm FinFET," in *Proc. IEEE Radio Freq. Integr. Circuits Symp.*, 2020, pp. 263–266.

[37] B. Welp et al., "Versatile dual-receiver 94-GHz FMCW radar system with high output power and 26-GHz tuning range for high distance applications," *IEEE Trans. Microw. Theory Techn.*, vol. 68, no. 3, pp. 1195–1211, Mar. 2020.

FLORIAN VOGELSANG (Graduate Student Member, IEEE) was born in Hattingen, Germany, in 1993. He received the B.Sc. and M.Sc. degrees in electrical engineering and information technology from Ruhr University Bochum, Bochum, Germany, in 2015 and 2017, respectively. He has been a Research Assistant with the Institute of Integrated Systems, Ruhr University Bochum, since 2018. His research interests include wideband radar systems in the mm-Wave and THz range, realized as monolithic microwave integrated circuits (MMIC) in silicon–germanium technologies.

JONATHAN BOTT (Graduate Student Member, IEEE) was born in Lünen, Germany. He received the B.Sc. and M.Sc. degrees in electrical engineering and information technology from TU Dortmund University, Dortmund, Germany, in 2014 and 2016, respectively. From 2016 to 2017, he worked in the automotive industry as a software developer. Since 2017, he has been a Research Assistant with the Institute of Integrated Systems, Ruhr University Bochum, Bochum, Germany. His research interests include mm-wave radar, monolithic microwave integrated circuit (MMIC) design using silicon–germanium, and MIMO algorithms.

DAVID STARKE (Graduate Student Member, IEEE) was born in Herne, Germany, in 1992. He received the B.Sc. and M.Sc. degrees in electrical engineering and information technology from Ruhr University Bochum, Bochum, Germany, in 2015 and 2017, respectively. Since 2017, he has been a Research Assistant with the Institute of Integrated Systems, Ruhr University Bochum. His research interests include mm-wave to THz radars and monolithic microwave integrated circuit (MMIC) design using silicon–germanium technologies.

CHRISTIAN BREDENDIEK (Member, IEEE) was born in Gelsenkirchen, Germany, in 1981. He received the Dipl.Ing. and Dr. Ing. degrees in electrical engineering from Ruhr University Bochum, Bochum, Germany, in 2008 and 2014, respectively. From 2008 to 2014, he was a Research Assistant with the Institute of Integrated Systems, Ruhr University Bochum. Since 2015, he has been with the Department of Integrated Circuits and Sensor Systems, Fraunhofer Institute for High Frequency Physics and Radar Techniques FHR, Wachtberg, Germany. His research interests include frequency synthesis, working on system concepts and integrated circuits for various mm-wave applications.

KLAUS AUFINGER (Member, IEEE) received the Diploma and Ph.D. degree in physics from the University of Innsbruck, Innsbruck, Austria, in 1990 and 2001, respectively. From 1990 to 1991, he was a Teaching Assistant with the Institute of Theoretical Physics, University of Innsbruck. In 1991, he joined the Corporate Research and Development of Siemens AG, Munich, Germany, where he investigated noise in submicrometer bipolar transistors. He is currently with Infineon Technologies AG, Neubiberg, Germany, the former semiconductor group of Siemens, Munich, working in the field of device physics, technology development, and modeling of advanced SiGe technologies for high-speed digital and analog circuits. He also gives lectures on analog bipolar technology at the Technical University of Munich, Munich. He has coauthored more than 200 publications in scientific journals and conferences. Dr. Aufinger was a member of the Technical Program Committee of the IEEE International Electron Devices Meeting (IEDM). He is a reviewer for several journals and the European Microwave Week (EUMW).

NILS POHL (Senior Member, IEEE) received the Dipl.-Ing. and Dr.-Ing. degrees in electrical engineering from Ruhr University Bochum, Bochum, Germany, in 2005 and 2010, respectively. From 2006 to 2011, he was a Research Assistant with Ruhr University Bochum, where he was involved in integrated circuits for millimeterwave (mm-Wave) radar applications. In 2011, he became an Assistant Professor with Ruhr University Bochum. In 2013, he became the head of the department of mm-wave radar and high frequency sensors with the Fraunhofer Institute for High Frequency Physics and Radar Techniques, Wachtberg, Germany. In 2016, he became a Full Professor of integrated systems with Ruhr University Bochum. He has authored or coauthored more than 200 scientific papers and has issued several patents. His research interests include ultra-wideband mm-wave radar, design, and optimization of mm-wave integrated SiGe circuits and system concepts with frequencies up to 300 GHz and above, and frequency synthesis and antennas. Dr. Pohl was the recipient of the Karl-Arnold Award of the North Rhine-Westphalian Academy of Sciences, Humanities and the Arts in 2013, and IEEE MTT Outstanding Young Engineer Award in 2018. He was the co-recipient of the 2009 EEEfCom Innovation Award, Best Paper Award at EuMIC 2012, Best Demo Award at RWW 2015, and Best Student Paper Awards at RadarConf 2020, RWW 2021, and EuMIC 2021. He is a member of VDE, ITG, EUMA, and URSI.